Investigation of the ^{22}Ne$(p,\gamma)^{23}$Na reaction via $(^3$He,$d)$ spectroscopy

S. E. Hale,[1] A. E. Champagne,[1] C. Iliadis,[1] V. Y. Hansper,[1] D. C. Powell,[1] and J. C. Blackmon[2]
[1]*University of North Carolina at Chapel Hill, Chapel Hill, North Carolina 27599-3255*
and Triangle Universities Nuclear Laboratory, Durham, North Carolina 27708-0308
[2]*Physics Division, Oak Ridge National Laboratory, Oak Ridge, Tennessee 37831*
(Received 6 June 2001; published 3 December 2001)

States near the ^{22}Ne$+p$ threshold in ^{23}Na were investigated using the ^{22}Ne$(^3$He,$d)^{23}$Na reaction over the angular range of $5°\leqslant\theta_{\rm lab}\leqslant 35°$ at $E(^3\mathrm{He})=20$ MeV. Spectroscopic factors were extracted for states corresponding to resonances in the ^{22}Ne$(p,\gamma)^{23}$Na reaction. Two previously suggested resonances at $E_{\rm c.m.}=68$ and 100 keV were not observed at any angle. A new rate for the ^{22}Ne$(p,\gamma)^{23}$Na reaction has been calculated and its implications are discussed.

DOI: 10.1103/PhysRevC.65.015801 PACS number(s): 25.10.+s, 26.35.+c, 28.20.−v, 98.80.Ft

I. INTRODUCTION

To first order, globular clusters are coeval, chemically homogeneous groups of stars and thus provide a good testing ground for theories of stellar evolution. However, closer scrutiny reveals interesting chemical effects. For example, observations of anticorrelations between sodium and oxygen [1–5] point to a more complicated situation than described by current stellar models, in which surface abundances should not change as the stars ascend the red-giant branch. Indeed, between the first dredge up (as the stars leave the main sequence) and the second dredge up (after core helium burning), these abundances should be unaltered. Observed variations in the surface abundances of carbon and nitrogen have led to the idea that nonconvective mixing, perhaps driven by rotation, is at work in these stars [6]. A possible byproduct of this augmented mixing is a change in the surface abundance of sodium (as well as helium) on the red-giant branch [7–9].

Nuclear physics provides circumstantial evidence to support the mixing picture. At high temperatures, leakage out of the carbon-nitrogen-oxygen (CNO) cycles into the NeNa cycle (Fig. 1) would have the effect of producing sodium while oxygen is destroyed. Although the flow from the CNO cycles to the NeNa cycle is negligible at low temperatures, it is possible to produce sodium from existing neon while oxygen is processed into other CNO nuclei, resulting in an apparent Na-O anticorrelation. However, some key reactions are known to be uncertain. The reaction that forms sodium in the NeNa cycle, ^{22}Ne$(p,\gamma)^{23}$Na, is thought to be dominated by numerous resonances above the (p,γ) threshold at 8794 keV (as shown in Fig. 2) and perhaps by direct capture at low energies. The direct-capture contribution has been measured by Rolfs *et al.* [10] and by Görres *et al.* [11]. However, the resonance component has not been accurately determined. As many as 14 states lie between threshold and the lowest-measured resonance at an excitation energy $E_x=9211$ keV (corresponding to $E_{\rm c.m.}=417$ keV [12]). On the basis of energetics, these states should be the most important resonances at the temperatures of interest ($T\leqslant 0.06\times10^9$ K or $T_9\leqslant 0.06$). Attempts have been made to populate these resonances directly [13] or via direct capture at higher energies [11], but none were observed. However, three of these states, at $E_x=8830$, 8945, and 8972 keV have been seen in the proton-stripping reactions $(^3$He,$d)$ [14] and (d,n) [15] and therefore could contribute to the ^{22}Ne$(p,\gamma)^{23}$Na reaction at some level. The $E_x=8822$-keV state has been observed via ^{19}F$(^6$Li,$d)^{23}$Na [16] with an angular-momentum transfer of five states. The resulting spin-parity assignment of $J^\pi=(9/2,11/2)^-$ implies h-wave transfer in ^{22}Ne$(p,\gamma)^{23}$Na and hence the proton width is negligibly small. Similarly, the state at 8799 keV is also too weak (because of its low energy) to contribute to the ^{22}Ne$(p,\gamma)^{23}$Na reaction. Of the remaining states, only those at 8862 and 8894 keV remain as potential contributors. These two states, along with the 9000-keV state, were reported to be weakly populated in the ^{22}Ne$(^3$He,$d)^{23}$Na reaction by Powers *et al.* [14],who concluded that their existence should be considered as tentative. Unfortunately, if they exist as resonances at $E_{\rm c.m.}=68$ and 100 keV, then they could contribute greatly to the reaction rate.

A reevaluation of the existing data was performed by El Eid and Champagne [17], in which it was found that the two tentative resonances produce large uncertainties in the reaction rate. Despite the uncertainty, the ^{22}Ne$(p,\gamma)^{23}$Na reaction is sufficiently fast to convert all ^{22}Ne to ^{23}Na within a typical burning time, *under steady-state conditions*. In contrast, the mixing scenario implies that the NeNa cycle operates episodically on a given mass element and here an uncertainty in the rate of ^{22}Ne$(p,\gamma)^{23}$Na will result in a similar uncertainty in the final abundance of ^{23}Na. At the same time, these resonances are low in energy and would be difficult to

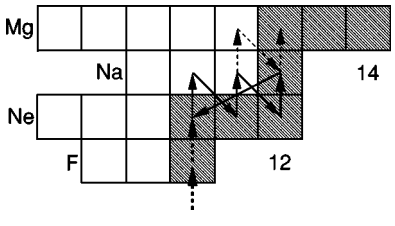

FIG. 1. Integrated fluxes from the CNO cycles up through the NeNa cycle. For the purpose of illustration, we have chosen $T_9=0.05$ and $\rho=100$ g/cm^3. Strong flows are indicated by heavy lines and weak flows are represented by dashed lines. Stable nuclei are represented by shaded boxes.

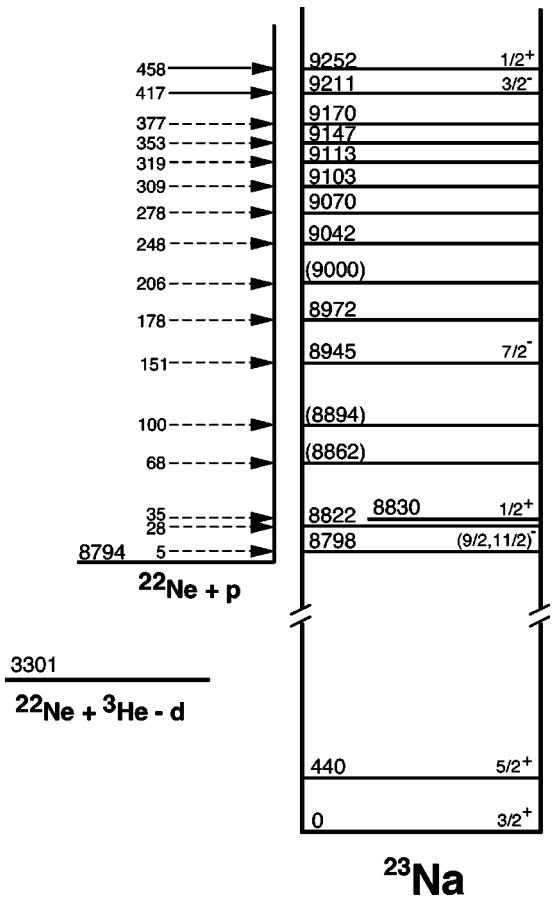

FIG. 2. Energy level diagram for ^{23}Na showing the location of known states and the predicted resonance energies. The excitation energies are taken from Ref. [12], while the Q value (8794.1 ± 0.3 keV) and the resonance energies have been recalculated using the 1995 mass evaluation [19].

detect directly, even at their maximum allowed strengths. However, the strengths of resonances near the proton-capture threshold are proportional to their proton widths. This latter quantity can be calculated if the proton spectroscopic factors are known. Consequently, we have reexamined the states near the ^{22}Ne$+p$ threshold using the ^{22}Ne(^{3}He,d)^{23}Na reaction in an effort to determine more precise proton widths, thus leading to a more accurate rate for the ^{22}Ne$(p,\gamma)^{23}$Na reaction at low temperatures. We have also reevaluated the existing energies and resonance strengths for resonances between $E_{\mathrm{c.m.}}=417$ and 1823 keV in order to refine the reaction rate at higher temperatures.

II. EXPERIMENTAL PROCEDURE AND RESULTS

A. Targets

The ^{22}Ne targets used in this study were produced by implanting singly charged ^{22}Ne ions into 40 μg/cm^2 $^{\mathrm{nat}}$C foils. To prevent accumulated stresses from rupturing the foils during implantation, they were first slackened by exposing them to a hand-held camera flash unit at a distance of 7 cm. The foils were placed in a target chamber, directly behind a graphite collimator with a defining aperture of 1.27 cm. This was done so that carbon would be the only material sputtered onto the foil as a consequence of beam collimation. In addition, the carbon sputtered onto the target foil is thought to increase the lifetime of the foil during the implantation process [18]. A copper tube extended to within 2 cm of the target holder. It was cooled to liquid-nitrogen temperature in order to reduce the buildup of contaminants on the target, and biased to -90 V for suppression of secondary electrons from the target. Beam current was read off the electrically insulated endpiece. The back end of the target holder contained a Plexiglas viewport to allow visual inspection of the back of the target throughout the implantation.

TABLE I. ^{22}Ne implantation doses.

Target side	Energy (keV)	Target #1 Dose (μA hr)	Target #2 Dose (μA hr)
Front	40	2.4	0.9
	20	4.0	4.1
Back	40	2.5	2.6
	20	3.4	4.4

Implantation was performed at energies of 20 and 40 keV using the Department of Physics and Astronomy ion implanter at the University of North Carolina. Each side of the C foil was exposed to the beam. This, and the two energies, spread the ^{22}Ne throughout the foil, which helped to maximize the amount of neon deposited. Beam currents were limited to 1.3 μA at 20 keV and 650 nA at 40 keV in order to keep the thermal stress within allowable limits. Three implanted ^{22}Ne targets were made and were evaluated for resolution and count rate by examining several states that are strongly populated by the ^{22}Ne(^{3}He,d)^{23}Na reaction. The two best targets were retained for data collection. The final beam-current exposures for these targets are listed in Table I.

B. Experimental details

A 20-MeV ^{3}He^{2+} beam was provided by the Triangle Universities Nuclear Laboratory FN tandem accelerator. Typical beam currents were between 100 and 150 pnA. The outgoing deuterons were momentum analyzed with the TUNL Enge Split-Pole Spectrometer and detected using a 42-cm long position-sensitive avalanche counter. The solid angle of the spectrometer was fixed at 2.0 msr in order to reduce the widths of the contaminant lines arising from carbon and oxygen in the target. Data were collected from $\theta_{\mathrm{lab}}=5°$ to 22.5° in 2.5° steps and from 25° to 35° in 5° steps.

The target was monitored using a $\Delta E-E$ silicon telescope, mounted in the target chamber at $\theta_{\mathrm{lab}}=44.2°$. The aperture of the monitor telescope was measured using a calibrated ^{241}Am source and found to be $d\Omega=0.92\pm0.01$ msr, consistent with a geometric measurement of 0.9 ± 0.1 msr. The yield from elastic-scattering measured with the monitor was also used to determine the absolute cross-section scale for the (^{3}He,d) data.

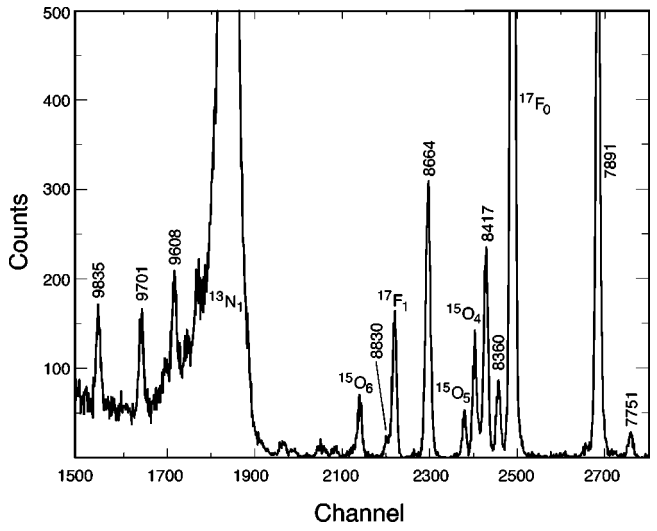

FIG. 3. Deuteron spectrum at $\theta_{\rm lab}=10°$. The peaks are labeled by either their energy in ^{23}Na in keV or by the final state formed from a contaminant in the target.

III. DATA ANALYSES

A. Excitation energies

A sample deuteron spectrum collected at $\theta_{\rm lab}=10°$ is shown in Fig. 3. In order to extract yields and centroids, the deuteron groups were fit with a template consisting of a Gaussian shape with a low-energy exponential tail. The magnitude and the slope of the two shapes were matched at a value of $X_{centroid}-1.4\sigma$, where $X_{centroid}$ is the Gaussian mean and σ is the normal Gaussian standard deviation. The value of 1.4 was determined by fitting three isolated deuteron peaks in each of the 5°, 10°, and 20° spectra with this template, and then varying the fitting point to minimize the χ^2 value of the fit.

The energy dispersion of the focal plane was calculated using the well-known energies of states populated in the ^{27}Al $(^3{\rm He},d)^{28}$Si reaction. This information was then used to calculate the difference in deuteron energies between the states of interest and the 8664-keV state in ^{23}Na. The resulting uncertainty in the excitation energies for states between the (p,γ) threshold and $E_x=9257$ keV was about 4 keV at all angles. The adopted excitation energies (shown in Table II) are a weighted average of the present results and all previous data, which were updated to take account of changes in tabulated masses [19].

TABLE II. Adopted excitation energies.

	E_x (keV)	
This study	Literature[a]	Adopted
8830±3	8829.5±0.7	8829.5±0.7
8946±3	8945±3	8945±2
8973±3	8972±3	8972±2
9044±3	9041±2	9042±1
9215±3	9211.3±0.8	9211.3±0.9
9257±3	9252.6±0.8	9252.1±0.9

[a]Reference [12].

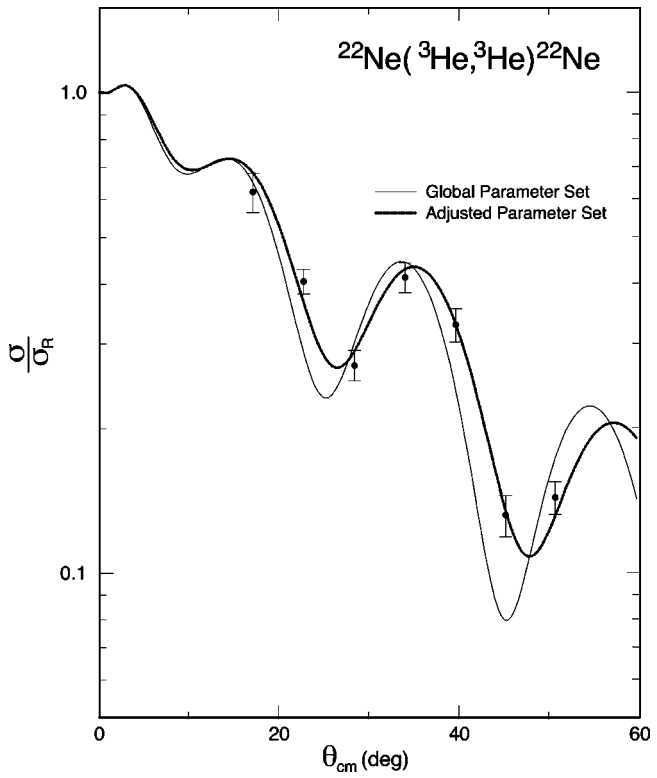

FIG. 4. The ratio of the differential cross section for ^{22}Ne(^{3}He,^{3}He)^{22}Ne to that for Rutherford scattering. The fits are DWBA calculations using different optical-model parameters, as described in the text.

B. Angular distributions

Absolute cross sections were determined by comparing the elastic-scattering yield measured using the monitor detector with (^{3}He, ^{3}He) angular-distribution data collected over the angular range of 15°–45° in steps of 5°. Theoretical differential cross sections were calculated with the distorted-wave Born approximation (DWBA) code DWUCK4 [20]. The ^{22}Ne+^{3}He potential parameters were initially taken from the global parametrization of Becchetti and Greenlees [21]. However, it was found that small modifications of individual parameters greatly improved the fit to the data (Fig. 4) and these new parameters were adopted for all of the DWBA calculations. The final ^{3}He parameters are given in Table III.

Deuteron optical-model parameters were surveyed by calculating differential cross sections for six states outside of the region of interest [from the (p,γ) threshold to the 417-keV resonance], which included the bound states at $E_x=7751$, 7891, and 8664 keV, and the unbound states at 9608, 9701, and 9835 keV. The relationship between the measured differential cross section, $d\sigma/d\Omega_{\rm expt}$ and that calculated by DWUCK4, $d\sigma/d\Omega_{\rm DWBA}$ is

$$\left(\frac{d\sigma}{d\Omega}\right)_{\rm expt}=N\frac{(2J_f+1)}{(2J_i+1)(2j+1)}C^2S\left(\frac{d\sigma}{d\Omega}\right)_{\rm DWBA}, \quad (1)$$

where $N=4.42$ is an overall normalization [22], J_f and J_i are the spins of the final and initial states, respectively, and j is the transferred total angular momentum. In this case, $j=l$

TABLE III. Optical-model parameters.

Particle	V_r	r_r	a_r	W_i	W_D	$r_i=r_D$	$a_i=a_D$	V_{so}	r_{so}	a_{so}	r_c
^{3}He[a]	162.2	1.05	0.72	44.89		1.33	0.86				1.30
d[b]	88.0	1.17	0.73	0.24	35.8	1.33	0.73	13.85	1.07	0.66	1.33
p[c]	[d]	1.17	0.69					$\lambda=25$			1.28

[a]From present elastic-scattering data.
[b]Reference [24].
[c]Reference [23].
[d]Varied to match separation energy.

$\pm 1/2$, where l is the transferred orbital angular momentum. We assumed $2s_{1/2}$, $2p_{3/2}$, $1d_{5/2}$, and $1f_{7/2}$ transfer. The quantity C^2S is the spectroscopic factor (the isospin Clebsch-Gordan coefficient $C^2=2/3$ for this combination of reaction and target). For unbound states, it is possible to extract the proton width, Γ_p via the relation

$$\Gamma_p = C^2 S \Gamma_{\rm sp}, \tag{2}$$

where $\Gamma_{\rm sp}$ is the calculated proton width for a pure single-particle state. A procedure for calculating $\Gamma_{\rm sp}$ is described by Iliadis [23]. These quantities are also calculated by DWUCK4 via

$$\Gamma_{\rm sp} = 2\left(\frac{d\delta}{dE}\right)^{-1}_{\delta=\pi/2} \approx \frac{\hbar^2 k}{\mu}\left[\int_0^{R_{max}} |u(r)|^2 dr + \frac{G^2}{2k}\frac{d}{dk}\left(\frac{G'}{G}\right)\right]^{-1}, \tag{3}$$

where δ is the phase shift, μ and k are the reduced mass and the wave number of the $A+x$ system, R_{max} is a cutoff radius at which the nuclear potential can be set to zero, G is the irregular Coulomb function evaluated at R_{max}, and $G' = (dG(r)/dr)_{r=R_{max}}$. The function $u(r)$ is the radial wave function calculated from the overlap of A and B in the theoretical $A(a,b)B$ cross section. The integration step size and R_{max} were arrived at by the requirement that variations in their values produced changes in $\Gamma_{\rm sp}$ of no more than 5%. The results calculated with this method are in agreement with those obtained using the parametrization found in Ref. [23]. We have chosen to express the differential cross section in terms of a spectroscopic factor (which is sensitive to the details of the nuclear potential) rather than with an asymptotic normalization coefficient (which is less sensitive by design) to facilitate comparison with previous results. This is simply an intermediate step. The quantity of interest is the proton width, which is insensitive to the choice of nuclear potential, and this is extracted directly from our angular-distribution data. Unbound form factors were calculated for the states above the ^{22}Ne$+p$ threshold.

The angular distributions for the six reference states are shown in Fig. 5. Satisfactory fits were achieved using deuteron potentials from the global parametrization of Daehnick *et al.* [24]. The only parameter that changed over the range of deuteron energies relevant for the present study has the magnitude of the volume-imaginary potential, which changed from 0.1 MeV to 0.4 MeV. This was too small to have a noticeable effect, and an average value of 0.24 MeV was adopted. Spectroscopic factors were obtained by a least-squares fit of the DWBA cross sections to the data and are listed in Table IV. The 1σ uncertainty in C^2S from the fit alone was about 3% for each state. The major systematic uncertainty in C^2S arises from ambiguities in the optical-model parameters. Since the absolute cross sections were determined relative to elastic scattering, C^2S is proportional to the ratio of the DWBA prediction for (^{3}He, ^{3}He) to that for (^{3}He,d), hence uncertainties in the ^{3}He parameters are

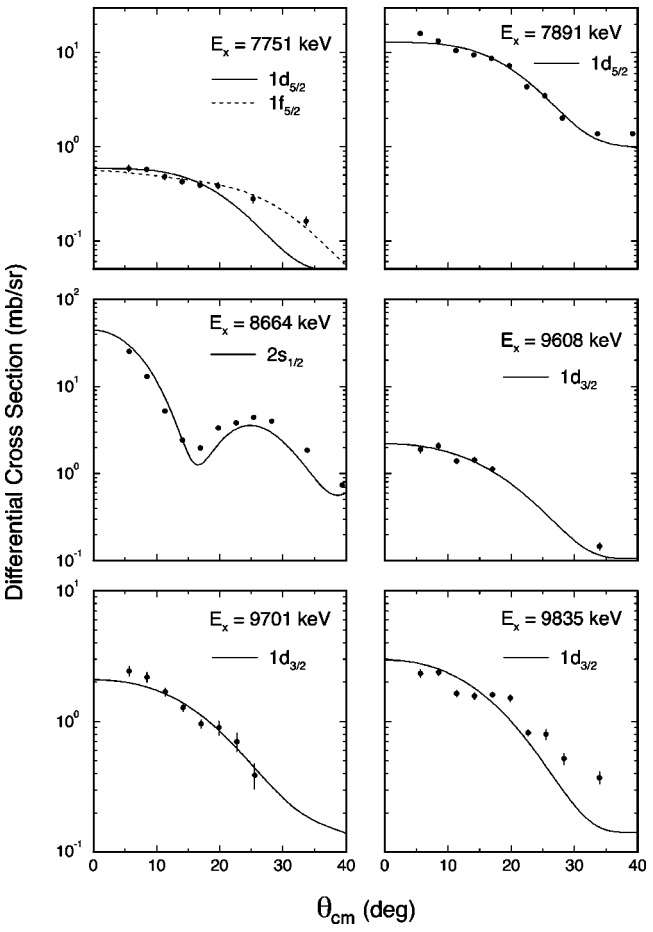

FIG. 5. Angular-distributions and DWBA fits for the six reference states. The error bars on the data points reflect statistical uncertainties only. The orbital angular-momentum transfer is noted for each fit.

TABLE IV. Summary of spectroscopic factors.

			$(2J_f+1)C^2S$	
E_x (keV)[a]	J^π [a]	l	This study[e]	Literature
7751	$\frac{5}{2}^+$	2	0.028	0.05[f]
	$\frac{5}{2}^-$[b]	3	0.076	0.084[g]
	$\frac{7}{2}^-$[b]	3	0.052	
	$\frac{7}{2}^+$	4	0.33	
7891	$\frac{5}{2}^+$	2	0.57	0.40[f]
				0.46[g]
8664	$\frac{1}{2}^+$	0	0.59	0.60 ± 0.08[h]
				0.50[f]
				0.54[g]
8830	$\frac{1}{2}^+$	0	0.039	0.036[g]
				0.08[f]
				0.054 ± 0.010[h]
8862	$\frac{1}{2}^+$[c]	0	$\leqslant 1.5\times10^{-3}$	$\leqslant 0.012$[h]
8894	$\frac{1}{2}^+$[c]	0	$\leqslant 1.6\times10^{-3}$	$\leqslant 0.030$[h]
8945	$\frac{7}{2}^-$	3	$\leqslant 8.7\times10^{-3}$	0.24[f], 0.012[g]
8972	$\frac{5}{2}^+$[c]	2	5.0×10^{-3}	7.0×10^{-3}[g]
	$\frac{7}{2}^-$[c]	3	9.2×10^{-3}	0.011[g]
9042	$\geqslant \frac{7}{2}^+$[d]	4	(0.02)	
9211	$\frac{1}{2}^+$[c]	0	0.02	
	$\frac{3}{2}^-$	1	3.9×10^{-3}	
9252	$\frac{1}{2}^+$	0	0.079	0.024[g]
9608	$\frac{3}{2}^+$	2	0.082	0.054[g]
9701	$\frac{3}{2}^+$	2	0.084	0.087[g]
9835	$\frac{3}{2}^+$	2	0.11	0.069[g]

[a]From Ref. [12] unless otherwise noted.
[b]From l transfer of present data and Ref. [14].
[c]Value derived from l of DWBA fit.
[d]From systematics of γ decay.
[e]The uncertainty in the present spectroscopic factors obtained from complete angular distributions is $\pm27\%$.
[f]Reference [15].
[g]Reference [14]. States above the proton-capture threshold have been reanalyzed using unbound form factors.
[h]Reference [11].

the major contributors to the overall uncertainty. To explore the effect of variations in these parameters, we have compared results obtained with the parameters listed in Table III to those obtained from the parameters of Ref. [21]. The average variation in the ratio $\sigma(^3\mathrm{He},{}^3\mathrm{He})/\sigma(^3\mathrm{He},d)$is 24%. Similar comparisons using different sets of deuteron parameters produce results that differ by about 11%. Treating all of these uncertainties as independent, Gaussian-distributed errors implies a total uncertainty of 27% for the spectroscopic factors reported here.

Proton widths were calculated for the three unbound states in our test sample and are listed in Table V along with

TABLE V. Proton widths of the reference states.

				Γ_p (eV)	
E_x (keV)	$E_{\mathrm{c.m.}}$ (keV)	J^π	l	$(^3\mathrm{He},d)$	(p,p)[a]
9608	813.4	$\frac{3}{2}^+$	2	6.3	3.4
9701	906.6	$\frac{3}{2}^+$	2	12.4	16.6
9835	1041.1	$\frac{3}{2}^+$	2	35.3	26.9

[a]Reference [25]. The typical uncertainty is $\pm50\%$.

experimental values determined from $^{22}Ne(p,p)^{22}Ne$ by Keyworth *et al.* [25]. Since they report uncertainties of about 50% for the widths of these states, the agreement with our results is adequate. However, we must also consider the uncertainties inherent in obtaining proton widths from stripping data. Clearly, the uncertainty in the spectroscopic factor contributes to the overall uncertainty, but uncertainties in optical-model parameters also enter into the calculation of Γ_{sp}. The value of Γ_{sp} depends on the matching of the internal wave function of the proton to the external Coulomb wave function and so it is quite sensitive to the nuclear potential. For example, 10% changes in radius or diffuseness produce a 40% change in Γ_{sp}. However, this also changes C^2S, but in the opposite direction. Thus the resulting change in Γ_p was less than 5% over this range of r_r and a_r. The fact that Γ_p is quite insensitive to the choice of potential parameters is to be expected since Γ_p is related to the probability that the incident proton will penetrate the Coulomb and centrifugal barrier to the nuclear surface. However, this interplay between C^2S and Γ_{sp} does make it difficult to estimate the uncertainty in Γ_p *a priori*. Thus, we have taken a phenomenological approach in which we have calculated the ratio of proton widths extracted from tabulated stripping data [12] to those obtained directly from (p,p) scattering for 35 resonances in the sd shell (specifically, in ^{24}Mg, ^{28}Si, and ^{32}S). We find a logarithmic mean of 0.95 with a logarithmic standard deviation of 1.76. Since we have taken the stripping data at face value and have not checked them for inconsistencies, the latter number may well be an overestimate. However, we will assume that the proton widths derived from our $(^3\mathrm{He},d)$ results carry an uncertainty of a factor of 1.8.

C. Results

We have observed six states in the region near the (p,γ) threshold, at $E_x=8830$, 8945, 8972, 9042, 9211, and 9252 keV. The latter two states correspond to the known $^{22}Ne(p,\gamma)^{23}Na$ resonances at $E_{\mathrm{c.m.}}=417$ and 458 keV. Angular-distributions and associated DWBA fits are displayed in Fig. 6. This region of the spectrum was obscured by contaminant groups arising from ^{14}N and ^{16}O in the target. Consequently, it was only possible to extract limited angular distributions, with the exception of that for the 8830-keV state. However, as will be seen below, this state is the only major contributor to the reaction rate below $E_{\mathrm{c.m.}}=417$ keV. No direct evidence for states at 8862 and 8894 keV was seen in the present study. A closer inspection of the spectrum displayed in Powers *et al.* [14] indicates that any

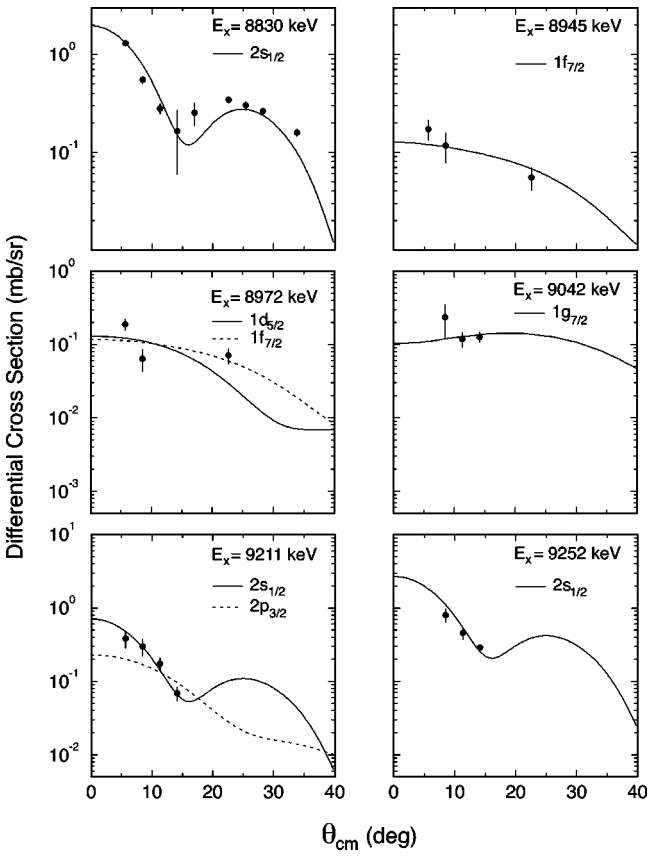

FIG. 6. Angular-distributions and DWBA fits for the low-energy states of interest. The orbital angular-momentum transfer is noted for each fit.

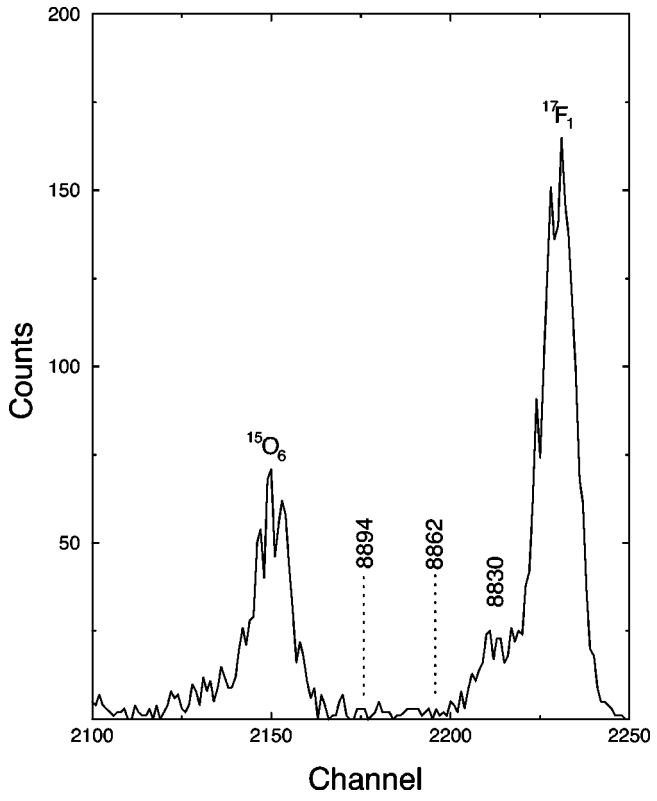

FIG. 7. A portion of the deuteron spectrum at $\theta_{\rm lab}=10°$ displaying the region of interest for the two possible states at 8862 and 8894 keV.

feature at the level of their background in the region of interest would have been readily discernable in our higher-dispersion, lower-background data. An example of the relevant region in our deuteron spectrum is shown in Fig. 7. A state at 8862 keV would have been clear of background at $\theta_{\rm lab}=10°$ and 12.5° whereas the 8894-keV state would be unobscured at 10°, 12.5°, and 15°. These angles were examined in more detail by using a maximum-likelihood technique [26] (described in the Appendix) to establish upper limits for the yields of these states. The resulting angular distributions are shown in Fig. 8. The data were analyzed by assuming *s*-wave transfer for each state, and ignoring any compound and/or second-order direct amplitude. The spectroscopic factors that we have extracted for the threshold states are summarized in Table IV.

IV. ASTROPHYSICAL ASPECTS

A. General considerations

The thermonuclear reaction rate is $N_A\langle\sigma v\rangle$, where N_A is Avogadro's number and $\langle\sigma v\rangle$ is the thermally averaged product of total cross section and velocity (in the center of mass). The contribution from an isolated, narrow resonance at $E_{\rm c.m.}$ can be written as

$$\langle\sigma v\rangle=\left(\frac{2\pi}{\mu kT}\right)^{3/2}\hbar^2(\omega\gamma)_r\exp\left(-\frac{E_{\rm c.m.}}{kT}\right). \qquad (4)$$

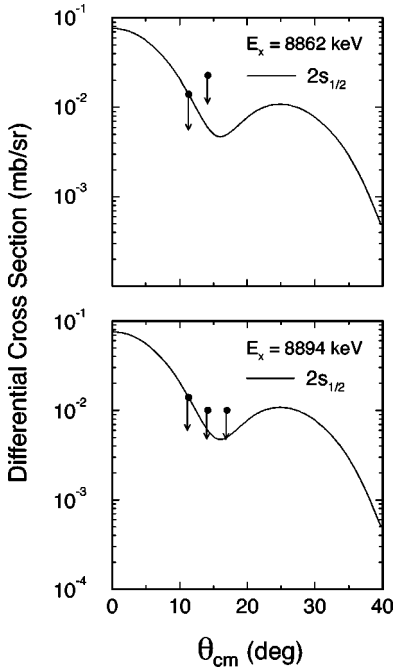

FIG. 8. Angular-distributions and DWBA fits for the two states at 8862 and 8894 keV. A spin parity $J^\pi=\frac{1}{2}^+$ was assumed for each state.

TABLE VI. Summary of resonance strengths.

E_x (keV)	$E_{\text{c.m.}}$ (keV)	J^{π}[a]	Γ_p (eV)	$\omega\gamma$ (eV) This study	$\omega\gamma$ (eV) Literature[f]	$\omega\gamma$ (eV) Adopted
8798	5		$\leqslant 2.1\times10^{-51}$ [d]	$\leqslant 2.1\times10^{-51}$		$\leqslant 2.1\times10^{-51}$
8822	28	$(\frac{9}{2}, \frac{11}{2})^-$	$\leqslant 5.4\times10^{-26}$	$\leqslant 3.2\times10^{-25}$		$\leqslant 3.2\times10^{-25}$
8829.5	35.4	$\frac{1}{2}^+$	3.6×10^{-15}	3.6×10^{-15}	6.8×10^{-15} [g]	3.6×10^{-15}
8862	(68)		$\leqslant 1.9\times10^{-10}$ [d]	$\leqslant 1.9\times10^{-10}$	$\leqslant 4.2\times10^{-9}$ [g]	$\leqslant 1.9\times10^{-10}$
8894	(100)		$\leqslant 1.4\times10^{-7}$ [d]	$\leqslant 1.4\times10^{-7}$	$\leqslant 6.0\times10^{-7}$	$\leqslant 1.4\times10^{-7}$
8945	151	$\frac{7}{2}^-$	$\leqslant 2.3\times10^{-9}$	$\leqslant 9.2\times10^{-9}$	6.5×10^{-7} [g]	$\leqslant 9.2\times10^{-9}$
8972	178		1.1×10^{-6} [e]	3.4×10^{-6}	$\leqslant 2.6\times10^{-6}$	$\leqslant 2.6\times10^{-6}$
9000	(206)				$\leqslant 1.4\times10^{-6}$	$\leqslant 1.4\times10^{-6}$
9042	248	$\geqslant \frac{7}{2}^+$ [b]	$\leqslant 3.2\times10^{-8}$	$\leqslant 1.3\times10^{-7}$	$\leqslant 2.6\times10^{-6}$	$\leqslant 1.3\times10^{-7}$
9070	278				$\leqslant 2.2\times10^{-6}$	$\leqslant 2.2\times10^{-6}$
9103	309				$\leqslant 2.2\times10^{-6}$	$\leqslant 2.2\times10^{-6}$
9113	319				$\leqslant 3.0\times10^{-6}$	$\leqslant 3.0\times10^{-6}$
9147	353				$\leqslant 6.0\times10^{-4}$ [h]	$\leqslant 6.0\times10^{-4}$
9170	377				$\leqslant 6.0\times10^{-4}$ [h]	$\leqslant 6.0\times10^{-4}$
9211	417	$(\frac{1}{2}^+$ [c], $\frac{3}{2}^-)$	0.42		0.65 [i]	0.65
9252	458	$\frac{1}{2}^+$	65		0.5 [i]	0.5

[a]From Ref. [12] unless otherwise noted.
[b]From systematics of γ decay.
[c]From present angular distribution.
[d]$2s_{1/2}$ transfer assumed.
[e]$1d_{5/2}$ transfer.
[f]From Ref. [13] unless otherwise noted.
[g]From Ref. [11].
[h]Estimate from Ref. [13] quoting excitation function of Ref. [27].
[i]From Ref. [31].

The quantity μ is the reduced mass, k is Boltzmann's constant, and $\omega\gamma$ is the resonance strength, defined by

$$\omega\gamma = \frac{2J_r+1}{(2J_t+1)(2J_p+1)}\frac{\Gamma_p\Gamma_\gamma}{\Gamma}, \tag{5}$$

in which J_r, J_t, and J_p are the spins of the resonance, target, and incident proton, respectively; and Γ_p, Γ_γ, and Γ are the proton and γ-ray partial widths, and the total width, respectively. At low-resonance energies, $\Gamma_p \ll \Gamma_\gamma$ and so the resonance strength reduces to

$$\omega\gamma \approx \frac{2J_r+1}{(2J_t+1)(2J_p+1)}\Gamma_p = \frac{2J_r+1}{2}C^2S\Gamma_{\text{sp}} \tag{6}$$

for the ^{22}Ne$(p,\gamma)^{23}$Na reaction. In the following, we will discuss the values that we have adopted for the strengths of the low-energy resonances.

B. Resonance strengths

In Table VI, we list the resonance strengths extracted from our spectroscopic factors. These results are discussed below.

1. E_x=8799 and 8822 keV, $E_{c.m.}$=5 and 28 keV

The 8799-keV and 8822-keV states were not observed in this study. However, as mentioned above, neither will make a significant contribution to the reaction rate because of low energy (for the former state) or high l transfer ($l=5$ for the latter state). For completeness, we have calculated resonance strengths by assuming $C^2S \leqslant 1$ for both states. The corresponding resonance strengths are $\omega\gamma \leqslant 2.1\times10^{-51}$ eV and $\omega\gamma \leqslant 3.2\times10^{-25}$ eV, respectively.

2. E_x=8830 keV, $E_{c.m.}$=35 keV

The 8830-keV state was observed previously in $(^3\text{He},d)$ [14] and (d,n) [15], with $(2J_f+1)C^2S=0.05$ and 0.08, respectively. However, both analyses have employed bound-state form factors. Consequently, we have reanalyzed the data of Powers *et al.* [14] using their potential parameters, but with unbound form factors and obtain $(2J_f+1)C^2S=0.036$. Although this is in good agreement with our value of 0.039, the quality of the fit is poor, indicating that their potential parameters have not been optimized. A measurement of the direct-capture contribution to the ^{22}Ne$(p,\gamma)^{23}$Na cross-section [11] reported $(2J_f+1)C^2S=0.054\pm0.010$. We have combined this value in a weighted average with our present spectroscopic factor to yield $(2J_f+1)C^2S=0.047\pm0.010$. This results in a resonance strength $\omega\gamma=3.6\times10^{-15}$ eV.

3. E_x=8862 and 8894 keV, $E_{c.m.}$=68 and 100 keV

The 8862-keV state was not populated in (p,γ) measurements ($\omega\gamma \leqslant 3.2$ μeV [13], $\leqslant 4.2$ neV [11]). The reanalysis of the available data by El Eid and Champagne [17] concluded that $\omega\gamma \leqslant 2.0$ neV. The upper limit on the resonance strength from the present work is more restrictive, $\omega\gamma(68\text{ keV}) \leqslant 0.19$ neV. Similarly, the upper limit on the

resonance strength for the 8894-keV state has been lowered as compared to the limits from the previous studies ($\omega\gamma \leqslant 0.6$ μeV [13], $\leqslant 5.6$ μeV [11], and $\leqslant 0.61$ μeV [17]). Our present value is $\omega\gamma(100\ \text{keV}) \leqslant 0.14$ μeV. The evidence that these states even exist is inconclusive at best. Therefore, our recommended reaction rate does not include a contribution from either state.

4. E_x=8945 keV, $E_{c.m.}$=151 keV

Based on the $l=3$ transfer seen in the (d,n) reaction [15] and the observation that this state decays 100% of the time to the $\frac{9}{2}^+$ state at 2704 keV [12], the 8945-keV state most likely possesses a J^π value of $\frac{7}{2}^-$. This state was also observed in $(^3\text{He},d)$ by Powers *et al.* [14], who remarked that the angular distribution seemed uncharacteristic of pure-l transfer (however, note that their Table III contains a misprint in which the spectroscopic factor for the 8972-keV state is reported as that of the 8945-keV state). Our limited angular distribution is not sufficient to establish an l transfer, but given $l=3$ transfer, we find $(2J_f+1)C^2S=8.7\times10^{-3}$ and a resonance strength of 9.2×10^{-9} eV. This strength is approximately a factor of 70.6 lower than what was calculated in Ref. [11], which was based on the much larger spectroscopic factor $[(2J_f+1)C^2S=0.24]$ reported from the (d,n) reaction [15]. However, the (d,n) data clearly show a sizeable compound-nuclear contribution to the cross section and the authors caution that their result might not be reliable. Our reanalysis of the $(^3\text{He},d)$ data of Powers *et al.* [14] yields $(2J_f+1)C^2S=0.012$, which is consistent with our result. However, the shape of their (more complete) angular distribution is not consistent with that of a pure, first-order direct process whereas our estimates of the spectroscopic factor and proton width are based on a one-step direct reaction. Thus, to be conservative we consider these quantities to be upper limits.

5. E_x=8972 keV, $E_{c.m.}$=178 keV

The 8972-keV state was also observed in the $(^3\text{He},d)$ measurements of Powers *et al.* [14] with an l transfer of either $l=2$ or 3, corresponding to $(2J_f+1)C^2S=7.0\times10^{-3}$ $(1d_{5/2})$ or 0.011 $(1f_{5/2})$, respectively (where again, we have reanalyzed their data using unbound form factors). Our angular-distribution data can only give a rough measure of the magnitude of the cross section. Assuming a pure $1d_{5/2}$ state, we obtain $(2J_f+1)C^2S=5.0\times10^{-3}$ and $\omega\gamma = 3.4$ μeV. This is larger than the limit set by Ref. [11] of 2.6 μeV. We have adopted the lower value. However, this state makes a negligible contribution to the reaction rate.

6. E_x=9000 keV, $E_{c.m.}$=206 keV

The tentative state at 9000 keV was reported by Powers *et al.* [14]. An upper limit of $C^2S\leqslant6\times10^{-3}$ was reported by Görres *et al.* [11] assuming $l=0$ transfer. This implies $\omega\gamma \leqslant 1.4$ μeV and a negligible contribution to the reaction rate.

7. E_x=9042 keV, $E_{c.m.}$=248 keV

The experimental situation regarding the 9042-keV state is similar to that encountered in the case of the 8972-keV state. Our limited angular-distribution data do not allow us to assign a unique l transfer. However, the lifetime and γ decay of this state have been tabulated [12] and we have made use of the criteria outlined there to obtain a most-probable spin assignment. Since this state decays to states with $J^\pi = 11/2^+ - 13/2^+$, $J^\pi=7/2^+$ is the minimum value consistent with the assertion that these decays are primarily $E2$ in character. Furthermore, the γ width derived from the lifetime is within the recommended upper limit for isoscaler $E2$ transitions. Thus, we adopt $J^\pi\geqslant7/2^+$, which implies $l\geqslant4$ transfer with $(2J_f+1)C^2S\approx0.02$ (for $l=4$). However, it is not clear if the assumption of a first-order direct process is valid. Several studies of the $^{12}\text{C}(^{12}\text{C},p\gamma)^{23}\text{Na}$ reaction indicate that the state is actually high-spin $(J^\pi\geqslant\frac{11}{2}^+)$ member of the $K^\pi = \frac{3}{2}^+$ ground state rotational band of ^{23}Na [28–30]. Consequently, we consider the resonance strength derived from our results, $\omega\gamma=0.13$ μeV, to be an upper limit. Note that this is more restrictive than $\omega\gamma\leqslant2.6$ μeV, reported in Ref. [11].

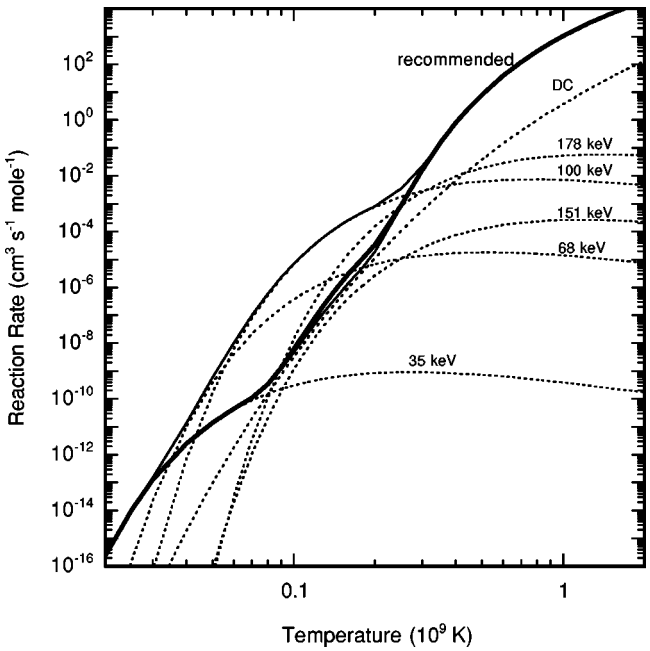

FIG. 9. Total reaction rate (solid lines), and individual contributions of resonances and direct capture (dashed lines) for the $^{22}\text{Ne}(p,\gamma)^{23}\text{Na}$ reaction. The upper and lower limits on the rate (with all [0-1] terms set to 1 or 0, respectively) are represented by the thin solid lines whereas the recommended rate is denoted by the heavy solid line.

8. E_x=9211 and 9252 keV, $E_{c.m.}$=417 and 458 keV

The strengths of the 417- and 458-keV resonances have been measured directly by Meyer and Smit [31]. The latter state is assigned $J^\pi=\frac{3}{2}^-$ in the compilation of Endt [12], whereas our fit favors $J^\pi=\frac{1}{2}^+$. A comparison of the values for the resonance strength (0.065 and 0.5 eV, respectively) with our proton widths (Table VI) reveals that the assumption $\Gamma_p\ll\Gamma_\gamma$ is no longer valid, but rather, the converse is true, i.e., $\Gamma_p\gg\Gamma_\gamma$. Consequently, the resonance strength is proportional to Γ_γ. Since we cannot derive resonance

strengths from our value for the proton width, we have used the results of Meyer and Smit [31].

9. $E_{c.m.} > 460$ keV

We have reevaluated the existing data [14,25,31–35] for resonances up to $E_{\text{c.m.}}=1823$ keV, which allows us to extend our calculation of the reaction rate to $T_9=2$. Where appropriate, we have used the latest tabulation of masses [19] to correct resonance energies. In cases where multiple measurements exist, the results were combined in a weighted average.

V. CONCLUSIONS

We have used Eq. (4) to calculate the individual reaction rates for all of the resonances surveyed here. An analytic expression for the total reaction rate is

$$\begin{aligned} N_A\langle\sigma v\rangle = {} & 1.05\times10^{9}T_9^{-2/3}\exp(-19.431/T_9^{1/3}) + 5.86\times10^{-10}T_9^{-3/2}\exp(-0.411/T_9) + 9.30\times10^{4}T_9^{-1.174} \\ & \times\exp(-5.100/T_9) + 5.71\times10^{5}T_9^{-0.249}\exp(-7.117/T_9) + [0-1]3.09\times10^{-5}T_9^{-3/2}\exp(-0.788/T_9) \\ & + [0-1]0.0228T_9^{-3/2}\exp(-1.159/T_9) + [0-1]1.50\times10^{-3}T_9^{-3/2}\exp(-1.752/T_9) \\ & + [0-1]0.423T_9^{-3/2}\exp(-2.065/T_9)\,\text{cm}^3\ \ \text{mole}^{-1}\ \ \text{sec}^{-1}. \end{aligned} \tag{7}$$

The first two terms include the contributions from direct-capture (from Ref. [11]) and the 35-keV resonance, respectively. The next two terms represent the resonances above 417 keV. The last three terms describe the upper-limit contributions from the 68-, 100-, 151- and 178-keV resonances, respectively. None of the possible resonances in the range $178\ \text{keV} < E_{\text{c.m.}} < 417$ keV make a significant contribution to the reaction rate and therefore their contributions are not included in Eq. (7). The total reaction rate and the individual contributions to it are shown in Fig. 9. We also display the rate in tabular form in Table VII. The upper and lower limits listed here include overall uncertainties of $\pm 40\%$ and $\pm 20\%$ associated with the direct-capture component and with the previously measured resonances ($E_{\text{c.m.}} > 417$ keV), respectively. We have also included our $1-\sigma$ systematic uncertainty of a factor of 1.8 in the strength of the 35-keV resonance. The uncertainty for direct capture was arrived at by combining the quoted 14% statistical uncertainty in the cross sections of Görres *et al.* [11] with our estimated uncertainties associated with their choice of optical-model parameters (27%) and fit (25%). The uncertainty for the known resonances is simply an approximation of the temperature dependent uncertainty in our weighted average of the resonance strengths. The rate that we recommend for use in nucleosynthesis calculations includes the first four terms of Eq. (7) and those for the 151- and 178-keV resonance, with the [0-1] factor set to 0.1. This latter resonance increases the reaction rate by less than 35% for $T_9=0.1$–0.25, which is in excess of the temperatures thought to be reached in low-mass red giants. Since there is no compelling evidence that the 68- and 100-keV resonances exist, we have not included them in the recommended rate.

Our recommended rate is significantly smaller than that appearing in the Nuclear Astrophysics Compilation of Reaction Rates (NACRE) compilation [36] for $T_9=0.03$–0.2. These rates are compared in Fig. 10. The primary reason for this difference is that our recommended strength for the 151-keV resonance has been reduced. This strength may still

TABLE VII. $^{22}Ne(p,\gamma)^{23}Na$ reaction rate.

T_9	Lower limit	Recommended	Upper limit
0.020	1.37×10^{-16}	2.46×10^{-16}	4.44×10^{-16}
0.025	5.97×10^{-15}	1.07×10^{-14}	1.95×10^{-14}
0.030	7.03×10^{-14}	1.27×10^{-13}	2.51×10^{-13}
0.040	1.40×10^{-12}	2.53×10^{-12}	1.60×10^{-11}
0.050	7.90×10^{-12}	1.42×10^{-11}	5.96×10^{-10}
0.060	2.46×10^{-11}	4.42×10^{-11}	1.06×10^{-8}
0.070	6.19×10^{-11}	1.10×10^{-10}	1.01×10^{-7}
0.080	1.73×10^{-10}	3.13×10^{-10}	5.87×10^{-7}
0.090	5.89×10^{-10}	1.19×10^{-9}	2.34×10^{-6}
0.100	2.10×10^{-9}	5.07×10^{-9}	7.07×10^{-6}
0.110	6.91×10^{-9}	2.02×10^{-8}	1.74×10^{-5}
0.120	2.04×10^{-8}	6.99×10^{-8}	3.65×10^{-5}
0.130	5.42×10^{-8}	2.09×10^{-7}	6.82×10^{-5}
0.140	1.31×10^{-7}	5.46×10^{-7}	1.16×10^{-4}
0.150	2.94×10^{-7}	1.28×10^{-6}	1.84×10^{-4}
0.160	6.20×10^{-7}	2.71×10^{-6}	2.76×10^{-4}
0.180	2.51×10^{-6}	9.96×10^{-6}	5.47×10^{-4}
0.200	1.10×10^{-5}	3.24×10^{-5}	9.62×10^{-4}
0.250	5.87×10^{-4}	8.50×10^{-4}	3.60×10^{-3}
0.300	1.30×10^{-2}	1.67×10^{-2}	2.54×10^{-2}
0.350	1.22×10^{-1}	1.54×10^{-1}	1.94×10^{-1}
0.400	6.48×10^{-1}	8.13×10^{-1}	9.90×10^{-1}
0.450	2.36×10^{0}	2.95×10^{0}	3.57×10^{0}
0.500	6.62×10^{0}	8.29×10^{0}	9.98×10^{0}
0.600	3.13×10^{1}	3.92×10^{1}	4.71×10^{1}
0.700	9.69×10^{1}	1.21×10^{2}	1.46×10^{2}
0.800	2.31×10^{2}	2.90×10^{2}	3.48×10^{2}
0.900	4.65×10^{2}	5.82×10^{2}	6.99×10^{2}
1.000	8.26×10^{2}	1.03×10^{3}	1.24×10^{3}
1.300	2.43×10^{3}	3.04×10^{3}	3.65×10^{3}
1.500	5.15×10^{3}	6.45×10^{3}	7.75×10^{3}
1.800	8.94×10^{3}	1.12×10^{4}	1.35×10^{4}
2.000	1.36×10^{4}	1.70×10^{4}	2.05×10^{4}

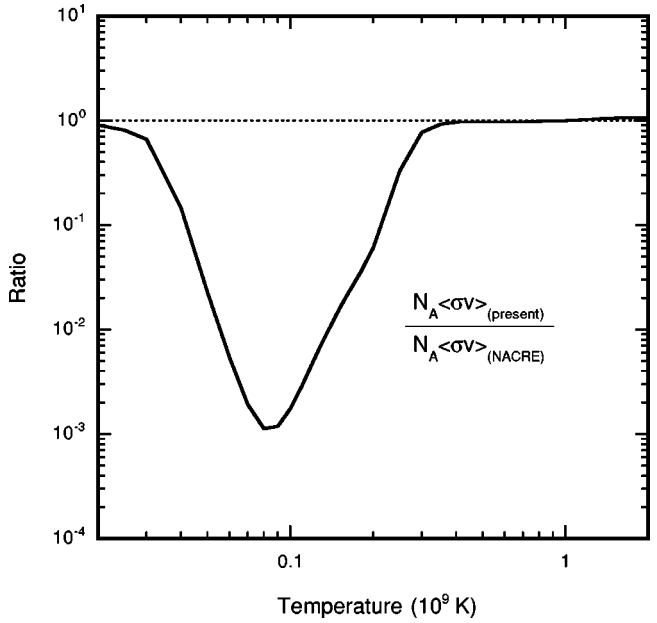

FIG. 10. Ratio of the present recommended rate to previous results [36].

be overestimated since the spectroscopic factor for this state is most likely an upper limit. However, since we have shown that this resonance contributes no more than 30% of the total reaction rate, the uncertainty about the structure of this state does not translate into a large uncertainty in the reaction rate.

We have significantly improved the accuracy of the ^{22}Ne$(p,\gamma)^{23}$Na reaction rate for temperatures characteristic of hydrogen burning in low-mass red giants. However, sizable uncertainties exist in the rates of the reactions that destroy ^{23}Na, ^{23}Na$(p,\gamma)^{24}$Mg, and ^{23}Na$(p,\alpha)^{20}$Ne, and these must be addressed before it will be possible to predict sodium abundances with improved stellar models. These reactions will be the subject of future work.

ACKNOWLEDGMENTS

This work was supported in part by U.S. DOE Grant No. DE-FG02-97ER41041.

APPENDIX: MAXIMUM-LIKLIHOOD ANALYSIS

To estimate upper limits on the number of counts associated with the 8862- and 8894-keV states, we have employed a maximum-likelihood estimation with Poisson statistics for both the possible foreground and the background, as described by Hannam and Thompson [26]. Their procedure finds the most likely signal (S) and background (B) strength in a specified region, given a template for each contribution. In this case, the signal shape was taken to be a Gaussian with a width equal to the average for the adjoining states and with a centroid predicted using the energy calibration at each angle. The background was taken to be linear, with a variable height. The mean number of counts in channel i, μ_i is

$$\mu_i = Bb_i + Ss_i, \tag{A1}$$

where b_i and s_i are the background and signal shapes, respectively. In this case, the most likely result is $S<0$, which corresponds to a physically unrealizable situation. Thus, the concept of a ΔS corresponding to a symmetric confidence belt loses its physical meaning. As a result, it was necessary to define a criterion for determining the upper limit on the number of counts, and hence the cross section. Unfortunately, there is no established convention on how this should be done (see, e.g., [37], The Review of Particle Properties [38] pages III 32 to III 42, [39], and references therein). The method chosen for this work was to renormalize the likelihood function such that the integral over the physical region ($S>0$) was equal to unity. The resulting new likelihood was then integrated up to the value of S at which 90% of the area is included. This was then interpreted as the upper limit at the 90% confidence level.

[1] R. P. Kraft, Publ. Astron. Soc. Pac. **106**, 553 (1994).
[2] R. P. Kraft, C. Sneden, G. H. Smith, M. Shetrone, G. E. Langer, and C. A. Pilachowski, Astron. J. **113**, 279 (1997).
[3] R. P. Kraft, C. Sneden, G. H. Smith, M. Shetrone, and J. Fulbright, Astrophys. J. **115**, 1500 (1998).
[4] J. E. Norris and G. S. Da Costa, Astrophys. J. **L81**, 441 (1995).
[5] C. A. Pilachowski, C. Sneden, R. P. Kraft, and G. E. Langer, Astron. J. **112**, 545 (1996).
[6] A. V. Sweigart and J. G. Mengel, Astrophys. J. **229**, 624 (1979).
[7] P. A. Denisenkov and S. N. Denisenkova, Sov. Astron. Lett. **16**, 275 (1990).
[8] G. E. Langer, R. Hoffman, and C. Sneden, Publ. Astron. Soc. Pac. **105**, 301 (1993).
[9] R. M. Cavallo, A. V. Sweigart, and R. A. Bell, Astrophys. J. **492**, 575 (1998).
[10] C. Rolfs, W. S. Rodney, M. H. Shapiro, and H. Winkler, Nucl. Phys. **A241**, 460 (1975).
[11] J. Görres, H. W. Becker, L. Buchmann, C. Rolfs, P. Schmalbrock, H. P. Trautvetter, A. Vlieks, J. W. Hammer, and T. R. Donoghue, Nucl. Phys. **A408**, 372 (1983).
[12] P. M. Endt, Nucl. Phys. **A251**, 1 (1990).
[13] J. Görres, C. Rolfs, P. Schmalbrock, H. P. Trautvetter, and J. Keinonen, Nucl. Phys. **A385**, 57 (1982).
[14] J. R. Powers, H. T. Fortune, R. Middleton, and O. Hansen, Phys. Rev. C **4**, 2030 (1971).
[15] W. A. Childs, R. C. Ritter, B. D. Murphy, and R. M. Strang, Nucl. Phys. **A203**, 133 (1973).
[16] H. T. Fortune, J. R. Powers, and L. Bargeron, Phys. Rev. C **51**, 1154 (1995).
[17] M. F. El Eid and A. E. Champagne, Astrophys. J. **451**, 298 (1995).
[18] L. K. Fifield and N. A. Orr, Nucl. Instrum. Methods Phys. Res. A **288**, 360 (1990).
[19] G. Audi and A. H. Wapstra, Nucl. Phys. **A595**, 409 (1995).
[20] P. D. Kunz, program DWUCK4 (unpublished), extended version

of J. R. Comfort (unpublished).
[21] F. D. Becchetti and G. W. Greenless, *Polarization Phenomena in Nuclear Reactions* (University of Wisconsin Press, Madison, 1971), p. 682.
[22] R. H. Bassel, Phys. Rev. **149**, 791 (1966).
[23] C. Iliadis, Nucl. Phys. **A618**, 166 (1997).
[24] W. W. Daehnick, J. D. Childs, and Z. Vrcelj, Phys. Rev. C **21**, 2253 (1980).
[25] G. A. Keyworth, P. Wilhjelm, G. C. Kyker, Jr., H. W. Newson, and E. G. Bilpuch, Phys. Rev. **176**, 1302 (1968).
[26] M. D. Hannam and W. J. Thompson, Nucl. Instrum. Methods Phys. Res. A **431**, 239 (1999).
[27] W. Heitzke, Ph.D. thesis, California State University, 1975.
[28] P. W. Green, G. D. Jones, D. T. Kelly, J. A. Kuehner, and D. T. Petty, Phys. Rev. C **12**, 887 (1975).
[29] B. B. Back, R. R. Betts, C. Gaarde, and H. Oeschler, Phys. Rev. C **13**, 875 (1976).
[30] G. J. KeKelis, A. H. Lumpkin, K. W. Kemper, and J. D. Fox, Phys. Rev. C **15**, 664 (1977).
[31] M. A. Meyer and J. J. A. Smit, Nucl. Phys. **A205**, 177 (1973).
[32] Z. B. du Toit, P. R. de Kock, and W. L. Mouton, Z. Phys. **246**, 170 (1971).
[33] C. E. Moss, Nucl. Phys. **A269**, 429 (1976).
[34] J. J. A. Smit, M. A. Meyer, J. P. L. Reinecke, and D. Reitmann, Nucl. Phys. **A318**, 111 (1979).
[35] E. L. Bakkum and C. van der Leun, Nucl. Phys. **A500**, 1 (1989).
[36] C. Angulo, M. Arnould, M. Rayet, P. Descouvemoont, D. Baye, C. Leclerq-Willain, A. coc, S. Barhoumi, P. Aguer, C. Rolfs, R. Kunz, J. W. Hammer, A. Mayer, T. Paradellis, S. Kossionides, C. Chronidou, K. Spyrou, S. Degl'Innocenti, G. Fiorentini, B. Ricci, S. Zavatarelli, C. Providencia, H. Wolters, J. Soares, C. Grama, J. Rahighi, A. Shotter, and M. Lamehi Rachti, Nucl. Phys. **A656**, 3 (1999).
[37] R. J. Barlow, *Statistics: A Guide to the Use of Statistical Methods in the Physical Sciences* (Wiley, Chichester, England, 1989).
[38] K. Hikasa *et al.*, Phys. Rev. D **45**, 32 (1992).
[39] G. Cowan, *Statistical Data Analysis* (Clarendon, Oxford, 1998).